Assessment of high-order DG methods for LES of compressible flows

By K. Hillewaert, J.-S. Cagnone†, S. M. Murman, A. Garai‡, Y. Lv AND M. Ihme

This paper describes validation work for high-order discontinuous Galerkin Methods on Large Eddy Simulation (LES) of canonical test cases including shocks, namely compressible homogeneous isotropic turbulence and homogeneous turbulence passing a shock. Three different DG methods are considered, and the impact of their shock-stabilization mechanisms is evaluated, as a preliminary step towards defining an optimized strategy.

1. Introduction

When performing DNS and LES of flows containing shocks, there is a delicate balance between the numerical dissipation necessary to bound the Gibbs phenomenon, and the low dissipation and dispersion mandatory for an accurate representation of the turbulent flow phenomena. Recently there has been heightened interest in the development of discontinuous-Galerkin (DG) methods because of their potential utility for industrial LES. While these methods have been evaluated on DNS and LES of canonical low-speed cases, rigorous evaluation for shock-turbulence interaction has been limited. Following investigations performed at the Stanford Center for Turbulence Research (CTR) by Larsson & Lele (2009) and Johnsen *et al.* (2010), the present research strives to close this gap by examining the behavior of high-order DG methods on canonical free-stream shock-turbulence test cases. The study involves three different DG methods. Argo, developed at Cenaero, is based on a standard high-order spatial DG discretization and method-of-lines time-integration; Eddy, developed at NASA Ames, uses a fully implicit, entropy-stable space-time scheme and finally, the entropy-bounded DG scheme of Stanford University.

2. Computational framework

The discontinuous Galerkin method (DG) (see Cockburn (1999)) is a Galerkin finite element method which seeks an approximate solution $\tilde{u} \approx u$ in a broken interpolation space $\mathcal{V}$, composed of functions $\tilde{v}$ that are polynomials of degree p on each of the elements in the mesh that are not required to be continuous across any of the element interfaces. After approximation of the solution by expansion in a convenient basis for $\mathcal{V}$, the expansion weights are found by requiring that the residual of the model equations, evaluated with $\tilde{u}$, be orthogonal to any function $\tilde{v} \in \mathcal{V}$. Owing to solution discontinuities, flux contributions appear on the element interfaces, which are functions of the left and right values and gradients of both solution u and test functions $\tilde{v}$. Borrowing ideas from unstructured finite volume solvers, the interface flux contributions of convective terms typically use upwind fluxes, whereas Arnold *et al.* (2002) summarize the different formulations possible for the diffusive contributions. As LES is, by definition, underresolved

† Cenaero, Belgium
‡ NASA Ames Research Center

and therefore inevitably features solution discontinuities, both interface terms, and in particular the convective flux, are deemed to have an important impact.

The method provides $\mathcal{O}(h^{p+1})$ accuracy in the L_2 error norm, excellent dispersion and dissipation properties, and a very low sensitivity to mesh quality. This precision, in combination with excellent strong scalability and computational efficiency, has provided the impetus for developing this method for practical, industrial scale-resolving simulations.

2.1. *Argo*

Argo uses a standard discontinuous Galerkin combined to a symmetric interior penalty formulation, with optimal penalty weights as derived by Hillewaert (2013). For this study 2p+3 accurate Gauss-Legendre quadrature is used. Argo was previously validated for DNS and LES on incompressible canonical test cases (Carton de Wiart *et al.* (2013); Carton de Wiart *et al.* (2014)) using conservative variables and the Roe approximate Riemann solver, which reflects the setup for this study. The shock-capturing approach follows that of Persson & Peraire (2006), where a small amount of artificial viscosity (AV) is used to regularize flow discontinuities towards a length scale resolvable by the interpolation space. The shock wave is located using a resolution indicator, which measures the relative energy of the p-th mode of the polynomial expansion in each element. Following the notation of the original reference, the baseline artificial viscosity ϵ_0 is chosen in the range $0.01 - 0.02$, whereas the detector threshold s_0 and the smoothing interval κ are -2 and 2, respectively.

2.2. *Eddy*

Eddy is a space-time discontinuous-Galerkin spectral-element solver. The discretization uses piecewise polynomials of arbitrary order formulated to take advantage of tensor-product bases and has been validated up to 16th order in both space and time. The compressible Navier-Stokes equations are discretized using an entropy variable formulation which discretely satisfies the second law of thermodynamics under exact integration. Integration is performed using 2N quadrature points in each coordinate direction for an Nth-order accurate solution. The inviscid flux is computed using the entropy stable flux of Ismail & Roe (2009), while the viscous fluxes are computed using an interior penalty method where the penalty parameter is consistent with the second method of Bassi and Rebay (BR2) (see again Arnold *et al.* (2002)). The non-linear system for each space-time slab is solved using a Jacobian-free approximate Newton-Krylov scheme preconditioned using diagonalized ADI. A detailed description is provided in Diosady & Murman (2015).

2.3. *The Stanford DG code*

The DG solver developed at Stanford supports a variety of DG formulations with modal or nodal bases, a collection of Riemann solvers, and two different diffusion discretization methods (interior penalty and BR2 schemes). Combined with an explicit RK scheme, the Stanford DG solver is capable of enforcing physical realizability of the numerical solutions with the aid of the entropy-bounded DG scheme detailed in Lv & Ihme (2015). Furthermore, the shock-capturing capability has recently been extended with an entropy-residual based shock detector and an artificial viscosity formalism described in Lv *et al.* (2016). In this present study, the entropy-bounded DG scheme is proven to be essential for numerical stability. Without such treatment, calculations for the compressible turbulence cases diverge. For the reported cases, the tensor-product Gauss quadrature that can exactly integrate polynomials of order 2N is employed, and the standard RK45 scheme is used for time integration. The Rusanov flux was used as an interface flux.

3. Compressible homogeneous isotropic turbulence

The first case concerns the transient and decay of transonic homogeneous isotropic turbulence in a triply periodic box as proposed by Johnsen *et al.* (2010). The flow is initialized with an incompressible flow field, such that a rather violent transient is encountered. The Reynolds number based upon the initial Taylor microscale λ_0 and rms of the velocity fluctuations $u_{rms,0}$ is $\mathrm{Re}_\lambda = u_{rms,0}\lambda_0/\nu = 100$. The initial turbulent Mach number $\mathrm{M}_t = \sqrt{3}u_{rms,0}/a = 0.6$ is sufficiently high to generate shocklets.

3.1. *Computational setup*

The DG computations were run at the same spectral resolution of 64^3 as the LES in the original paper. In order to approximate the baseline resolution of 64^3, the number of cells was divided by p+1 (corresponding to the number of degrees of freedom in each direction), hence 16, 13, 11 and 8 cells, respectively, were used in each direction for interpolation orders p=3,4,5 and 7. Argo was deployed with and without shock capturing. The Stanford code was used in the standard version, including the entropy bounding, which proved to be indispensible in this case. Both teams considered interpolation orders p=3, 4 and 5, combined with RK4 time-stepping. The Eddy computations were undertaken at a single resolution of 64^3, interpolation orders 7 (space) and 3 (time). All computations used a sufficiently small time step (CFL<0.1) such that only the spatial error remains.

3.2. *Comparisons to the original paper*

Figure 1 illustrates the time evolution of the volume-averaged kinetic energy $\mathcal{K}$ and enstrophy $\mathcal{E}$, defined in terms of velocity $\mathbf{v}$ and vorticity ω as

$$\mathcal{K} = \frac{1}{2V}\int_V \mathbf{v}\cdot\mathbf{v}\; dV \;,\; \mathcal{E} = \frac{1}{2V}\int_V \omega\cdot\omega\; dV. \tag{3.1}$$

These results are compared to the filtered reference DNS by Johnsen *et al.* (2010). In these graphs, time is non-dimensionalized by $\tau = \lambda_0/u_{rms,0}$ and the other quantities as indicated in the axis legend. All DG codes follow the evolution of total kinetic energy much better than in the reference paper, whereas enstrophy seems systematically overestimated. However, note that the DNS reference solution was filtered to the LES resolution 64^3. As we expect the enstrophy to be significantly reduced by filtering, it was not clear whether these higher values are actually wrong, and thus new DNS were performed using CharLES (256^3) and Argo (p=5, 384^3) to provide upper reference values. Most of the DG results proved to be quite close to the non-filtered DNS, whereas almost all codes in Johnsen *et al.* (2010) provide values below even the filtered DNS, even for kinetic energy. In the following section, we provide data indicating that for the given resolution, very good resolution is obtained at 64^3, at least for the energy statistics.

Figure 2 compares the RMS of the temperature fluctuations and dilatation $\theta = \nabla\cdot\mathbf{v}$. We notice first that the new DNS provides slightly smaller temperature fluctuations than the original filtered DNS in Johnsen *et al.* (2010), which is unexpected. As for enstrophy, we find that the filtering operation has an important impact on the dilatation. Furthermore, there is a small discrepancy between the DNS computations with Argo and CharLES. All codes underpredict the peak occurring around $t/\tau = 0.6$, and then maintain too high a level of divergence for the remainder of the computation.

3.3. *Energy balance*

Using the momentum equation and the periodicity of the domain, the dissipation $\mathcal{W}$ of the density-weighted kinetic energy consists of the viscous dissipation $\mathcal{W}_d$ (which is

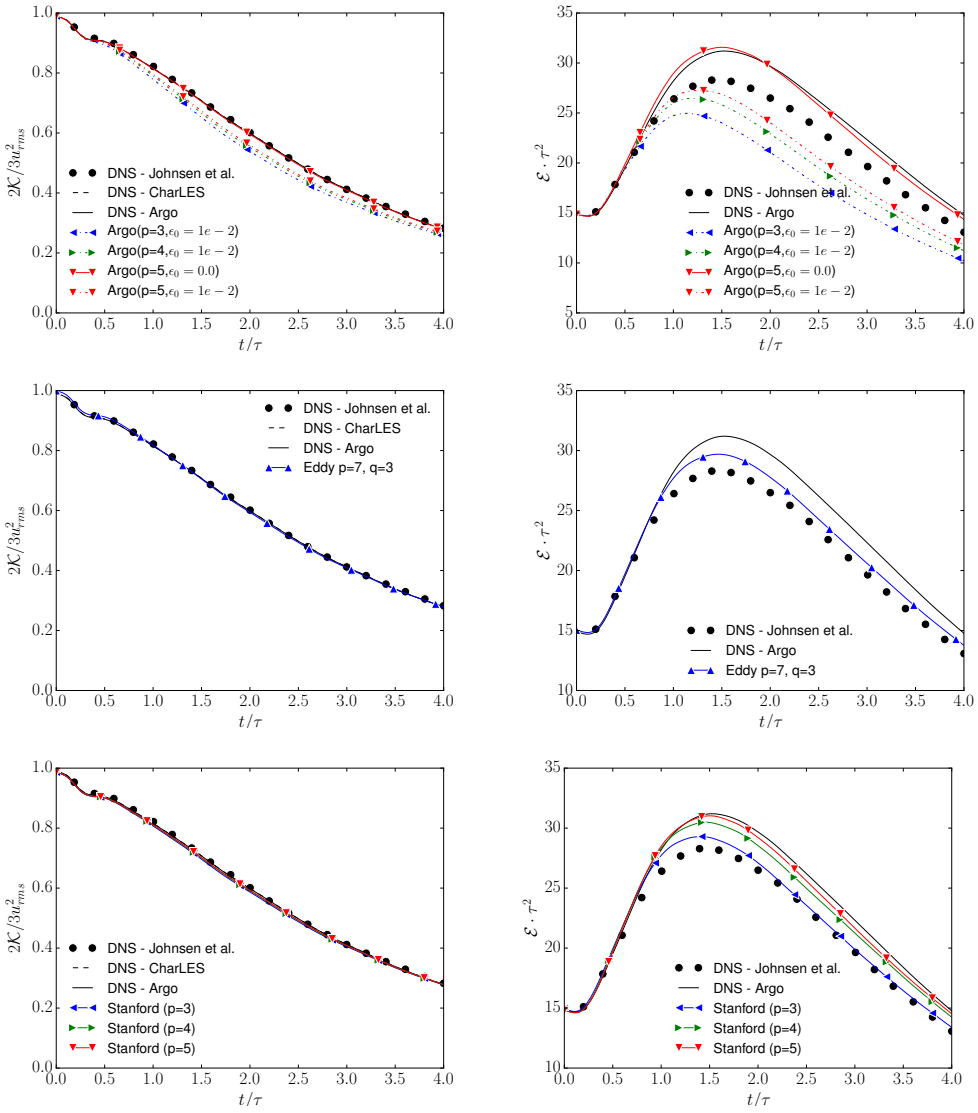

FIGURE 1: Compressible HIT: time evolution of kinetic energy (left) and enstrophy (right) for Argo (top), Eddy (middle) and the Stanford DG code (bottom).

$\mathcal{W} = 2\mu\mathcal{E}$ for incompressible flow) and the pressure work $\mathcal{W}_c$

$$\underbrace{-\frac{d}{dt}\left(\frac{1}{2}\int_V \rho\mathbf{v}\cdot\mathbf{v}\;dV\right)}_{\mathcal{W}} = \underbrace{\int_V \left(2\mu\boldsymbol{S}:\boldsymbol{S} - \mu_d\left(\nabla\cdot\mathbf{v}\right)^2\right)dV}_{\mathcal{W}_d} - \underbrace{\int_V p\nabla\cdot\mathbf{v}\;dV}_{\mathcal{W}_c}, \tag{3.2}$$

with the usual definitions for the shear stress $\boldsymbol{\sigma} = \mu\boldsymbol{S} - \mu_d(\nabla\cdot\mathbf{v})\boldsymbol{I}$ and strain deviatoric tensor $\boldsymbol{S} = \frac{1}{2}\left(\nabla\mathbf{v} + \nabla\mathbf{v}^T\right)$. Obviously, this relation is only approximately satisfied by the discretized equations. We then define the measured dissipation $\widetilde{\mathcal{W}_m}$ as the time derivative of the discrete density-weighted kinetic energy and the theoretical dissipation $\widetilde{\mathcal{W}_t}$ as the

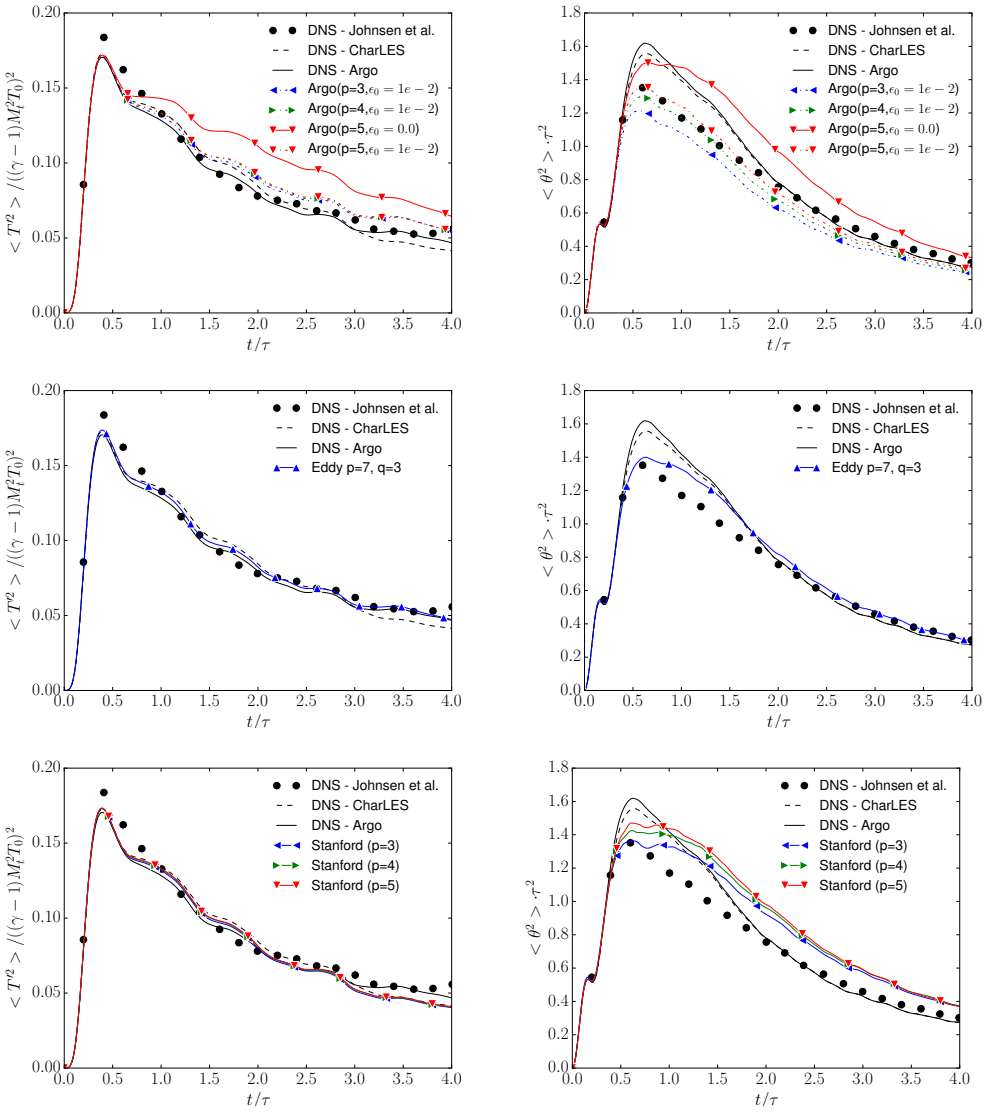

FIGURE 2: Compressible HIT: time evolution of the rms values of dilatation (left) and temperature fluctuations (right) for Argo (top), Eddy (middle) and the Stanford DG code (bottom)

sum of the viscous dissipation $\widetilde{\mathcal{W}_d}$ and the pressure work $\widetilde{\mathcal{W}_c}$, both evaluated with the discrete solution. The difference $\widetilde{\mathcal{W}_t} - \widetilde{\mathcal{W}_m}$ is then a direct error measure. Figure 3 collects a representative set of results. All terms are non-dimensionalized with $\mathcal{W}^* = \mu/\tau^2$. For the DNS we see a perfect match between both measured and theoretical dissipation. The initial acoustic imbalance provides a very important transient, in particular for $t/\tau < 1$.

The Argo code is not consistently stable, and often crashes around $t/\tau = 0.6 - 0.7$. In fact, no computations were successfuly completed without shock capturing for the two lowest orders (p=3 and 4), while many fewer problems are encountered with p=5.

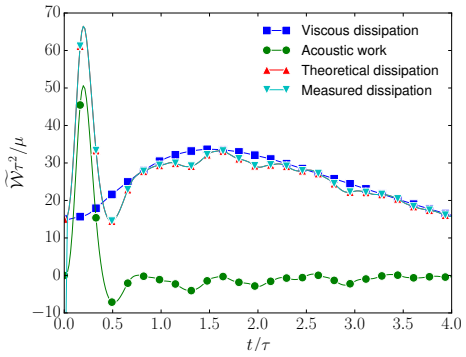

(a) DNS Argo p=4 384^3

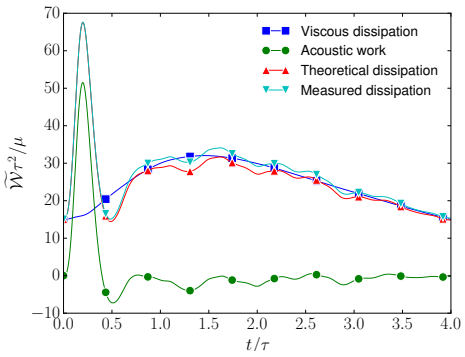

(b) Eddy p=7, temporal order 3

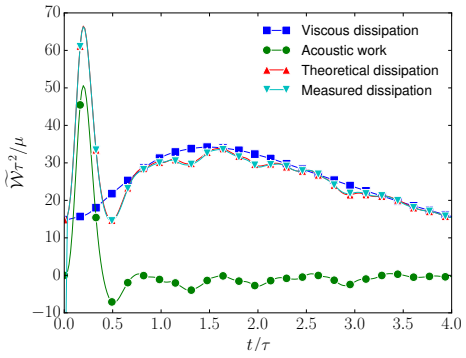

(c) Argo p=5, no shock capturing

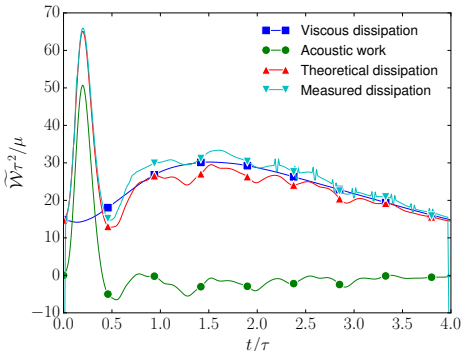

(d) Stanford solver p=4

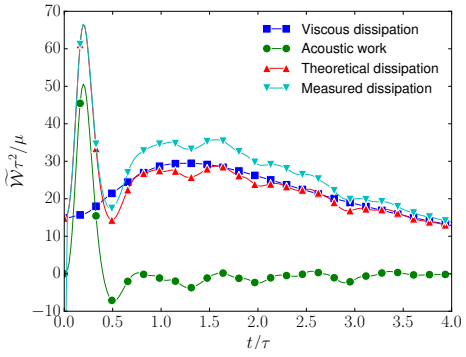

(e) Argo p=5, shock capturing $\epsilon_0 = 0.01$

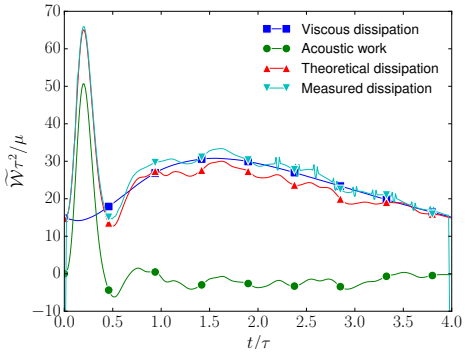

(f) Stanford solver p=5

FIGURE 3: Compressible HIT: dissipation balances.

This apparent increase of robustness with interpolation order is contrary to common experience for LES. This result can probably be attributed to the unexpectedly high resolution obtained at 64^3. In these conditions, higher orders result in improved capture of the physics, which then reduces overshoots and undershoots. The addition of artificial viscosity $\epsilon_0 = 10^{-2}$ stabilizes all computations, at the cost of a significant loss of precision. This simple approach is clearly not adequate and needs to be improved for this test case.

Similarly, in the case of the Stanford code, we find that the entropy-bounding mechanism has an important impact on the energy balance, in particular on viscous dissipation, similar to the differences seen in enstrophy. The mechanism seems more selective than the shock capturing used in Argo, but from p=4 onwards, the results do not improve with order, indicating that the stabilization is partly triggered by the physics.

Only a single computation was performed with Eddy at p=7, with no discernible problems. A small but noticeable deficit in the energy balance can be seen, in particular with respect to viscous dissipation. This discrepancy is unexpected, as the computation should, *a priori*, be more precise than the Argo results which were obtained with a lower polynomial order. This could be due to a slight inconsistency in the evaluation of the different terms with the space-time discretization, or the use of a coarser time resolution. This aspect is currently under investigation. Although the entropy conservation built into Eddy is definitely an asset, the code was run at p=7 and conclusions cannot be drawn on the basis of this test case alone. Coarser computations are still needed to evaluate the accuracy of the formulation for truly underresolved compressible turbulence.

4. Homogeneous isotropic turbulence passing through a shock

The next case consists of freestream turbulence interacting with a shockwave. Currently, the test case has been run using Argo only. We focus on two inflow Mach numbers, $\mathrm{M} = 1.28$ and $\mathrm{M} = 1.5$, chosen from the study of Larsson & Lele (2009) whose DNS serves as reference data. The computational domain is a box of dimension $[4\pi \times 2\pi \times 2\pi]$, with periodic boundary conditions in the transverse (y and z) directions. The simulations are carried-out on two grid densities, containing 192×64^2 and 384×128^2 interpolation points repectively, clustered near the shock location. We note that Larsson & Lele (2009) used 1040×384^2 grid points to achieve DNS accuracy, implying that the present calculations have LES resolution at best. The simulations are implicitly integrated with a time-step of $k_0 u_{1,u} \Delta t \approx 0.06$, and the flow statistics are accumulated over $k_0 u_{1,u} t_{\mathrm{stat}} \approx 180$, where the notation $u_{1,u}$ indicates the upstream value of the first component of the velocity.

As in the original paper, the inflow turbulence is extracted from a precursor simulation of homogenous isotropic turbulence (HIT), initiated with a divergence-free velocity field with an exponentially-decaying spectrum, a peak wavenumber of $k_0 = 4$, a turbulent Mach number of $\mathrm{M}_t = 0.33$ and a microscale Reynolds number of $\mathrm{Re}_\lambda = 140$. The turbulence is then evolved for three eddy turnover times, to reach $\mathrm{M}_t = 0.22$ and $\mathrm{Re}_\lambda = 40$. This solution is then rotated to obtain three independent turbulent realizations, which are blended using the method of Xiong *et al.* (2004). This blended database is scanned through to continuously provide the turbulent fluctuations superimposed on the nominal inflow condition. The outlet static pressure is adjusted to fix the shock position according to the procedure of Larsson & Lele (2009). In order to damp spurious reflections, the DG interpolation is reduced from cubic ($p = 3$) to piecewise-constant ($p = 0$) near the outlet, over a layer $x_{\max} - x_{p0} \approx \pi$.

Results obtained for Mach number $\mathrm{M} = 1.28$ are shown in Figure 4a. The streamwise and transverse Reynolds stress, $u_1' u_1'$ and $u_2' u_2'$, are normalized by their value upstream of the shock and then compared against the reference DNS data. These turbulent fluctuations are observed to first decrease monotonically, before rapidly increasing across the shock. The particularly large variations of the streamwise component is due to the unsteady shock motion which exacerbates the local fluctuations. After the increase through the shock, the Reynolds stresses recover their monotonically decreasing behavior, but

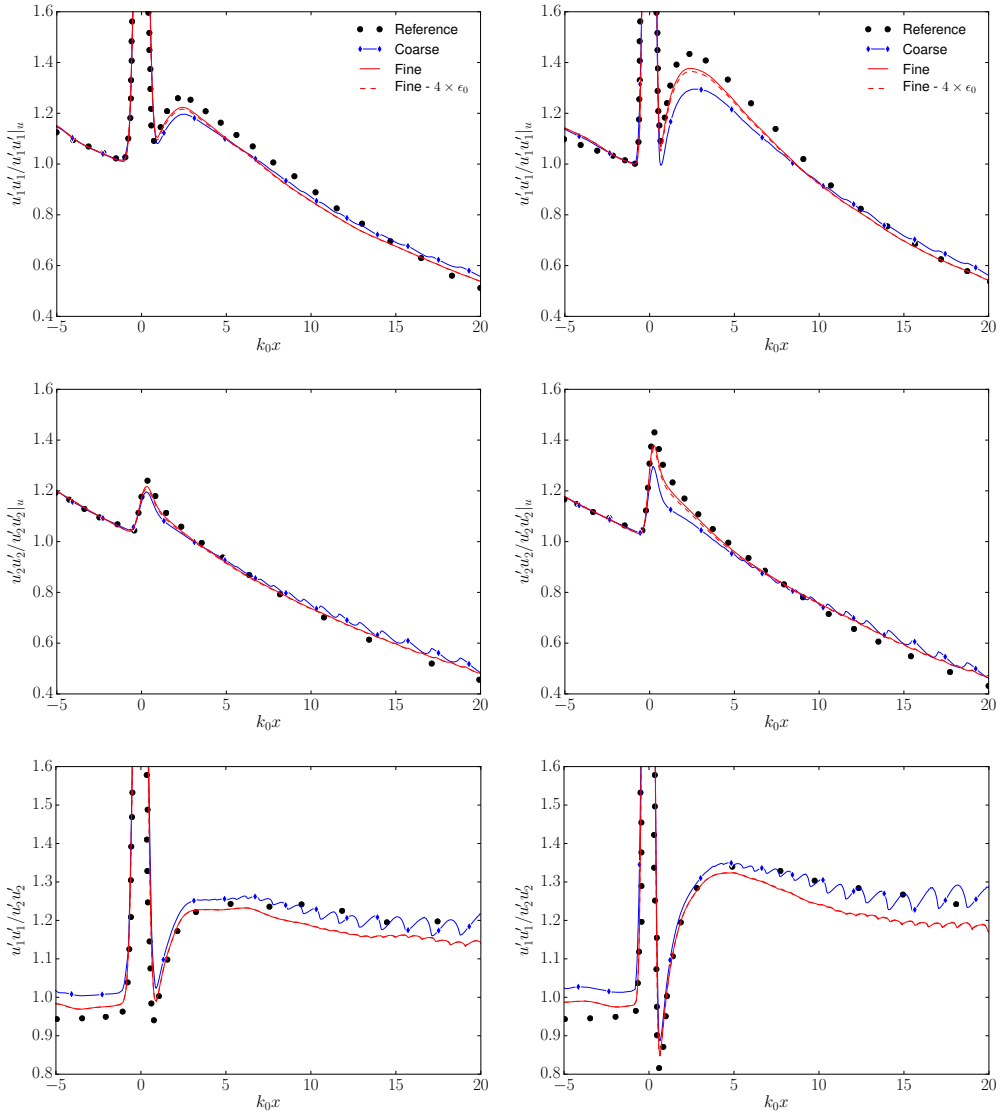

(a) $\mathrm{M} = 1.28, \mathrm{M}_t = 0.22$. (b) $\mathrm{M} = 1.5, \mathrm{M}_t = 0.22$.

FIGURE 4: Shock-turbulence cases: evolution of velocity correlations

the anisotropy observed in the streamwise-to-transverse fluctuations persists all the way to the outlet. From a quantitative standpoint, the present resolutions are confirmed as being too coarse to yield a point-to-point agreement with the DNS, with both coarse and fine solutions slightly underpredicting the post-shock fluctuations. However, the general solution behavior agrees adequately with the reference, and the expected Reynolds-stress anisotropy produced through the shockwave is reproduced. We note that our pre-shock anisotropy level does not exactly coincide with the DNS, and shows a dependence on the grid resolution. This discrepancy likely affects the shock-turbulence interaction, but its net impact is not discernible from mesh or numerical dissipation effects. Figure 4a

also shows an additional fine-grid calculation with the shock-capturing parameter ϵ_0 increased by a factor of four. Since the solution is effectively unchanged, we conclude that the shock-capturing is sufficiently localized as not to affect the time-averaged turbulent statistics.

Figure 4b shows the results for the second Mach number M = 1.5, for which the fluctuation rise across the shock is more pronounced. The overall agreement with the DNS is adequate, but a greater difference between the coarse and fine grids is observed. Concentrating on the coarse grid results, we remark that the increase in Reynolds stresses across the shock is underpredicted for both streamwise and transverse components. However, the anisotropy ratio is remarkably well predicted. We note that this systematic underprediction, consistent with the dissipative nature of the ILES-DG method, contrasts with the results obtained with finite-difference methodologies. In a study employing WENO schemes and explicit subgrid-scale models, Bermejo-Moreno *et al.* (2010) report that the streamwise and transverse components are, respectively, over- and underpredicted, thus failing to capture the post-shock anisotropy level. The dissipative behavior of the DG method, if confirmed on higher Mach cases, could prove thus advantageous for shock-dominated turbulent simulations. The applicability of the present scheme is further confirmed by the additional fine-grid calculation with increased AV. As for the previous case, the results show a very low dependence on the shock-capturing parameters, thus demonstrating the robustness and suitability of the present method.

5. Conclusions and perspectives

Three different discontinuous Galerkin methods were compared on a compressible isotropic turbulence test case. This effort is a first step towards a more complete assessment of DG, and potentially implicit LES, for compressible turbulent regimes. The emphasis was put on shock-stabilization mechanisms, and their impact on the accuracy of each scheme. A second test case concerning shock-turbulence interaction was performed, using Argo only.

We conclude that the DGM approaches have excellent resolving capabilities, in comparison to methods previously applied to the same cases. However, stabilization mechanisms such as artificial viscosity and entropy bounding have an important impact on the solution quality. In particular artificial viscosity is poorly suited for flow regimes in which the turbulence itself generates shocks, even if the mesh resolution *a priori* provides an adequate capture of the physics. Simultaneously, we also observe that the artificial viscosity approach seems adequate if the shock arises independently of the turbulence, as demonstrated on the shock-turbulence problem. For the HIT case, the stabilization is only required to pass a particularly severe transient caused by acoustic imbalances, and this stabilization could either be reduced or removed altoghter in more realistic senarios. The present DG computations compared very well with DNS, in terms of energy-balance preservation. However, the resolution employed is probably too fine for a true LES at the current Reynolds number Re_λ and further studies are needed on higher Re_λ, including cases without the initial unphysical transient.

Lastly, we note that filtering DNS results for validation of LES is a common practice. Although the motivation is straightforward, it is not clear which filtering is most appropriate, in particular for derivative quantities such as dissipation. In the current study, we have observed that a filtered DNS solution, initially intended for benchmarking finite-difference solvers, is not an appropriate reference for DG. We would therefore advocate

to systematically report the unfiltered DNS, in addition to the filtered data. However, further research is needed to develop robust filtering procedures, possibly tailored to the numerical method at hand.

Acknowledgments

The Argo computations were performed using computational resources made available on the Tier-1 supercomputer of the Fédération Wallonie-Bruxelles, infrastructure funded by the Walloon Region under the grant agreement #1117545.

REFERENCES

Arnold, D., Brezzi, F., Cockburn, B. & Marini, L. 2002 Unified analysis of discontinuous Galerkin methods for elliptic problems. *SIAM J. Numer. Anal.* **39**, 1749–1779.

Bermejo-Moreno, I., Larsson, J. & Lele., S. K. 2010 LES of canonical shock-turbulence interaction. *Proceedings of the summer program*, Center for Turbulence Research, Stanford University, pp. 209–222.

Cockburn, B. 1999 *Higher-order methods for computational physics*, In *Lecture Notes in Computational Science and Engineering*, vol. 9, chap. Discontinuous Galerkin Methods for Convection-Dominated Problems, pp. 69–224. Springer.

Diosady, L. T. & Murman, S. M. 2015 Higher-order methods for compressible turbulent flows using entropy variables. *AIAA Paper #2105-0294*.

Hillewaert, K. 2013 *Development of the Discontinuous Galerkin Method for high-resolution, large scale CFD and acoustics in industrial geometries.* PhD Thesis, Ecole Polytechnique de Louvain/iMMC.

Ismail, F. and Roe., P.L. 2009 Affordable, entropy-consistent Euler flux functions II: Entropy production at shocks. *J. Comput. Phys.* **228**, 5410–5436

Johnsen, E., Larsson, J., Bhagatwala, A. V., Cabot, W. H., Moin, P., Olson, B. J., Rawat, P. S., Shankar, S. K., Sjögreen, B., Yee, H., Zhong, X. & Lele, S. K. 2010 Assessment of high-resolution methods for numerical simulations of compressible turbulence with shock waves. *J. Comput. Phys.* **229**, 1213–1237.

Larsson, J. & Lele, S. K. 2009 Direct numerical simulation of canonical shock/turbulence interaction. *Phys. Fluids* **21**, 126101.

Lv, Y. & Ihme, M. 2015 Entropy-bounded discontinuous Galerkin scheme for Euler equations. *J. Comput. Phys.* **295**, 715–739.

Lv, Y., See, Y. C. & Ihme, M. 2016 An entropy-residual shock detector for solving conservation laws using high-order discontinuous Galerkin methods. *J. Comput. Phys.* **332**, 448–472.

Persson, P. & Peraire, J. 2006 Sub-cell shock capturing for discontinuous Galerkin methods. *AIAA Paper* #2006-112.

Carton de Wiart, C., Hillewaert, K., Bricteux, L. & Winckelmans, G. 2014 Implicit LES of free and wall bounded turbulent flows based on the discontinuous Galerkin/symmetric interior penalty method. *Int. J. Numer. Meth. Fl.* **78**, 335–354.

Carton de Wiart, C., Hillewaert, K., Duponcheel, M. & Winckelmans, G. 2013 Assessment of a discontinuous Galerkin method for the simulation of vortical flows at high Reynolds number. *Int. J. Numer. Meth. Fl.* **74**, 469–493.

Xiong, Z., Nagarajan, S. & Lele, S. K. 2004 Simple method for generating inflow turbulence. *AIAA J.* **42**, 2164–2166.